Distribution Agreement

In presenting this thesis as a partial fulfillment of the requirements for a degree from Emory University, I hereby grant to Emory University and its agents the non-exclusive license to archive, make accessible, and display my thesis in whole or in part in all forms of media, now or hereafter now, including display on the World Wide Web. I understand that I may select some access restrictions as part of the online submission of this thesis. I retain all ownership rights to the copyright of the thesis. I also retain the right to use in future works (such as articles or books) all or part of this thesis.

Arjun Vohra March 28th 2025

Characterization Of a Human Dorsal Root Ganglion Organoid Patterning Recipe

by

Arjun Vohra

Jimena Andersen

Adviser

Department of Biology

Jimena Andersen

Adviser

Fikri Birey

Committee Member

Andreas Fritz

Committee Member

2025

Characterization Of a Human Dorsal Root Ganglion Organoid Patterning Recipe

By

Arjun Vohra

Jimena Andersen

Adviser

An abstract of
a thesis submitted to the Faculty of Emory College of Arts and Sciences
of Emory University in partial fulfillment
of the requirements of the degree of
Bachelor of Science with Honors

Department of Biology

2025

Abstract

Characterization Of a Human Dorsal Root Ganglion Organoid Patterning Recipe

By Arjun Vohra

Human dorsal root ganglion (DRG) organoids derived from human induced pluripotent stem cells (hiPSCs) provide an *in vitro* model to study sensory neuron development and pain-related disorders. This study compared three DRG organoid recipes by varying the timing of 5-fluorodeoxyuridine (FUDR) application to arrest progenitor proliferation at different time points: Regular (d15, d22), Delayed (d29, d36), and No FUDR (No FUDR treatment). Because progenitor cells switch from neurogenesis to gliogenesis during development, arresting proliferation at different timepoints may interrupt one of these 2 processes, resulting in different proportions of glial cells and neurons (such as nociceptors, proprioceptors and mechanoreceptors) in the resultant organoids, which may be of consequence to modelling disease. Quantitative PCR (qPCR) revealed that neural progenitor markers for all recipes, such as *SOX10* peaked early, while glial markers such as *FABP7* and *GFAP* increased over time, which was consistent with model of DRG development reflecting the expected gliogenic switch. The Delayed FUDR condition showed significantly higher expression of *ISL1* (a neuronal marker) at d63, which might suggest extended neurogenesis. Microelectrode array (MEA) recordings at d120 showed higher baseline firing rates in the Delayed FUDR condition, supporting this claim. Exposure to capsaicin, a nociceptor agonist, showed no significant differences in capsaicin-induced responses across conditions, suggestive of low nociceptor activity. These results highlight how modifying FUDR timing alters cellular composition and activity in DRG organoids – the Delayed FUDR group was found to have increased neuronal activity and expression of neural markers relative to the other group, warranting further investigation into the precise mechanism why and other ways in which the functionality of this recipe may differ relative to the other groups.

Characterization Of a Human Dorsal Root Ganglion Organoid Patterning Recipe

By

Arjun Vohra

Jimena Andersen

Adviser

A thesis submitted to the Faculty of Emory College of Arts and Sciences
of Emory University in partial fulfillment
of the requirements of the degree of
Bachelor of Science with Honors

Department of Biology

2025

Table of Contents

Contents

Characterization Of a Human Dorsal Root Ganglion Organoid Patterning Recipe

1. Introduction

Given recent advances in the field of human induced pluripotent stem cell (hiPSC)-derived organoids as models for human neurodevelopmental and neurodegenerative disease, increased efforts to recreate more specific parts of the human central nervous system have resulted in a larger variety of patterned organoids. One region of interest is the dorsal root ganglion (DRG) due to its involvement in sensory perception of stimuli such as pain, making it of medical importance for studying conditions such as chronic pain and ataxia (Koeppen et al.). While historically other model organisms, such as mice, have been used to study this intersection of the peripheral and central nervous systems, studies have found differences between mouse and human DRG cell populations - one such example involves nociceptors, the somatosensory neurons that detect pain – analgesics that work in rodent models often fail in human trials (Shiers et al.). This could be a consequence of species-specific adaptations in nociceptors that result in divergent functions (Jung et al.). As such, developing an *in vitro* human model of the DRG may one day prove to be a complementary method of studying DRG related conditions, and is one of medical and pharmaceutical importance. In order to do so, it is essential to have a patterning recipe that is reliable and produces organoids that mimic the biological system *in vitro*. To gauge the optimal recipe, it must be compared with other alternatives. This paper aims to do that, with the goal of comparing three recipes that alter neurogenesis – an important process in the development of DRG – in differing ways.

1.1. Anatomy and microanatomy of the DRG

Before introducing the organoid model used in this study, the system which it is trying to recreate must first be introduced. The dorsal root ganglion is defined as a cluster of afferent sensory cell bodies linking the peripheral nervous system to the central nervous system through the spinal cord. These clusters are located at the dorsal root entry zone of the spinal cord at each vertebral level. They consist of pseudounipolar cell bodies, defined as a neuron with a single axon that divides into two processes: in the case of the DRG, the shorter process projects into the dorsal horn of the spinal cord, while the longer process innervates sensory receptors within tissue. Broadly speaking, there are three distinct types of sensory neurons located within the DRG: nociceptors, mechanoreceptors and proprioceptors, which are responsible for the detection of pain, physical touch and balance, respectively (Metzer et al.; Haberberger et al.). Thus, a signal originating in the peripheral nervous system, induced by some sensory stimulus, makes its way through the peripheral nervous system to the longer process, into the DRG soma, and then onwards into the spinal cord where it is processed by the central nervous system.

1.1.1. Non-neuronal cell populations of the DRG

Other than neurons, non-neuronal glial cells are also present in the DRG. The most abundant of these non-neuronal glial cells are called satellite glial cells (SGCs) which are specific to the DRG (Haberberger et al.). According to Haberberger et al., these cells affect the functionality of the DRG as they increasingly envelope the soma of neurons with age and play roles in modulating neural activity due to the presence of glutamate receptors –a neurotransmitter used by the sensory neurons. Additionally, Schwann cells are also present within the DRG, being derived from the Schwann cell precursor lineage of neural crest progenitor cells. Schwann cells likely play a role in affecting the functionality of the DRG: they have been linked responsible for inducing excitability

in developing DRG neurons via their secretion of prostaglandin PGE2 which induces sodium voltage-gated channel expression in the DRG (Kantarci et al.). Additionally, *in vivo*, Schwann cells induce myelination and pseudounipolarization in the developing DRG (Metzer et al.). Thus, the non-neuronal cells of the DRG also play a variety of different roles in its functionality.

1.2. Embryonic Development of the DRG

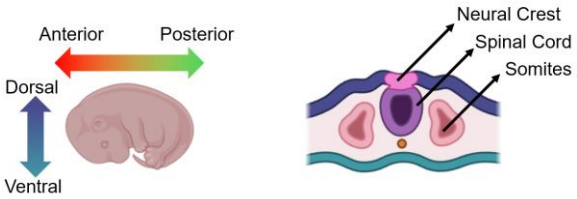

.

Figure 1. Developmental axes of the embryo (left) and cross section of a generic embryo during neurulation (right). Figure generated using BioRender.

Given that the adult DRG has been described, the mechanism by which this system develops is of particular importance to modelling it *in vitro*. The cells of the DRG, and indeed the cells of the nervous system in general, derive from the neuroectodermal lineage during embryonic development. The neural tube is a tube of neural progenitors which runs along the anterior-posterior axis of the embryo just under the dorsal ectoderm (**Fig 1A**). Following the development of this tube, neural crest progenitors (which comprise the dorsal side of the tube) undergo an epithelial-to-mesenchymal transition following which they migrate away from the tube in an anterior-posterior order. The ventral side of the tube remains in place and will form the spinal cord. The migration of these progenitor cells is regulated by the somites of an embryo, developmental segments of muscle progenitors running paraxially to either side of the developing spinal cord that will be innervated by the sensory neurons of the DRG. The DRG is specifically derived from the trunk neural crest lineage, which follows this general progression of differentiation: trunk neural crest, which differentiate into Schwann cell precursors, which may further differentiate into

enteric, parasympathetic and sympathetic neurons. Other fates of the trunk NCC include chromaffin cells and melanocytes (Alhashem et al.; Achilleos et al.).

1.2.1. Neurogenesis, gliogenic switch and excitability in nascent DRG *in vivo*

Once migrating DRG neural crest progenitors have coalesced to form condensed structures, they are believed to undergo neurogenesis in two overlapping waves: in mice, the first wave occurs from E9 to E10.5, which is linked to a rise in nociceptive neurons, while the second wave which lasts from E9.5 to E13, generates smaller diameter neurons such as proprioceptors and mechanoreceptors (Ma et al.; Wiszniak and Schwarz). Whether these waves of neurogenesis occur in distinct waves, and whether each wave gives rise to a distinct type of somatosensory neuron is debated, but this is the prevailing model (Metzer et al.). Glia differentiates after neurons – an irreversible gliogenic 'switch' occurs when neural crest progenitors are exposed to Notch signaling, which causes them to differentiate into glial fates (Morrison et al.). In humans, a study found that the first wave of neurogenesis occurs *in vivo* at gestational week (GW) 7 and ends at GW8 resulting in the differentiation of mechanoreceptors, the second wave occurs from GW7 to GW12 resulting in the differentiation of nociceptors. They found that GW12 represented the week at which the gliogenic switch occurred (Lu, et al.). In organoids, they found that the first wave of neurogenesis was largely complete by day 30, and that by day 60, the gliogenic switch had occurred (Lu, et al.).

During development, Kantarci et al. found that it is Schwann cells that are responsible for inducing excitability in developing DRG neurons via their secretion of prostaglandin PGE2 which induces sodium voltage-gated channel expression in the DRG. Additionally, according to Metzer, immature DRG sensory neurons are not pseudounipolar but instead poses a bipolar morphology with two spindles – projections to the spinal cord precede the adoption of the pseudounipolar

phenotype. Adding Schwann cells to cultured DRG neurons induces a mature pseudo-unipolar morphology in cultured tissue, though this has not been observed in organoids.

1.3. hiPSCs and Organoids

A human induced pluripotent stem cell (hiPSC) is the term used to refer to a patient-derived somatic cell that has been induced back into a pluripotent state through the introduction of reprogramming factors such as OCT4, SOX2, KLF4, and c-MYC. Such hiPSCs exhibit characteristics similar to embryonic human stem cells such as morphology, proliferation, feeder dependence, surface markers and gene expression (Ho et al.). An additional benefit of hiPSCs over embryonic stem cells lies in the fact that hiPSCs can be patient-derived – as such, should they be used to generate tissue, such tissue would have a low chance of rejection. Alternatively, they can be used to model diseases, as tissue derived from a diseased patient might exhibit characteristics of the disease. As such, hiPSCs present an attractive target for manipulation to model tissue and diseases. In order to do so, hiPSCs must be directed to differentiate into cell fates of interest. This process, known as patterning, involves exposing the cells to various small molecules and growth factors to guide cells into specific lineages by mirroring the patterning that occurs during embryonic development. While this has traditionally been done in two dimensions to a stem cell monolayer, this can now be done in three dimensions by first aggregating the cells into organoids. Such stem cell organoids, when patterned in three dimensions, exhibit multi-lineage differentiation resulting in heterogenous populations of cells that self-organize into more tissue-like architecture (Ho et al.).

1.4. hDRG patterning

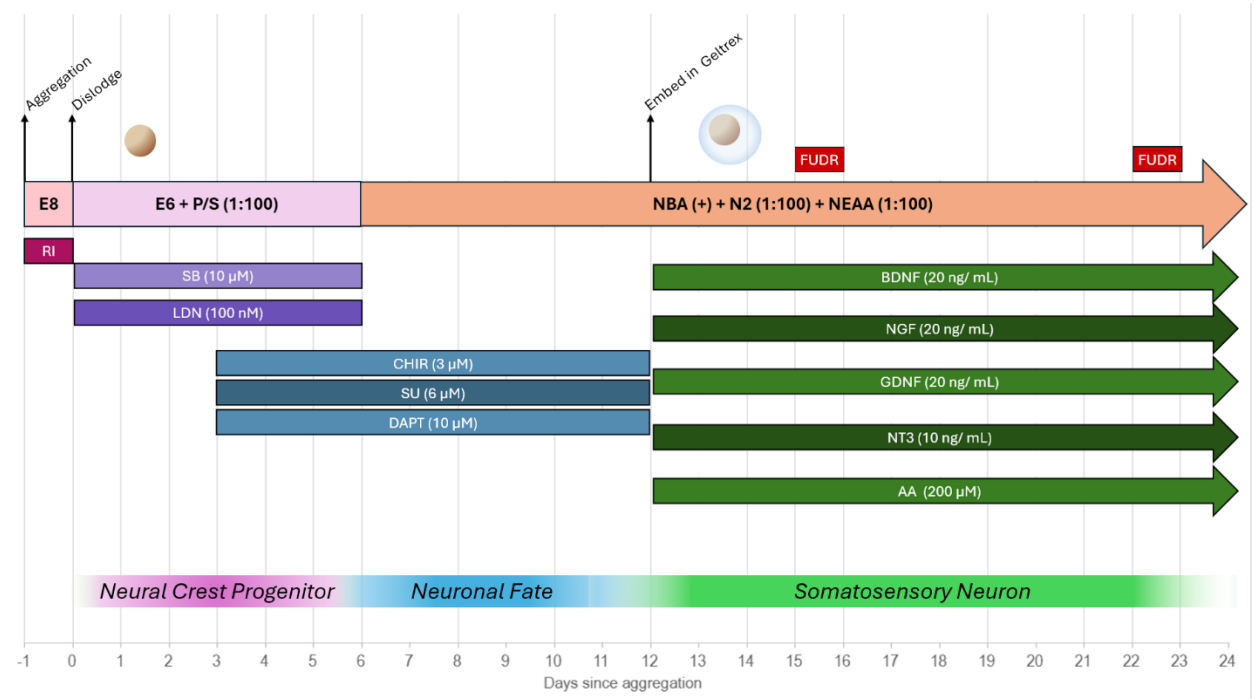

(A)

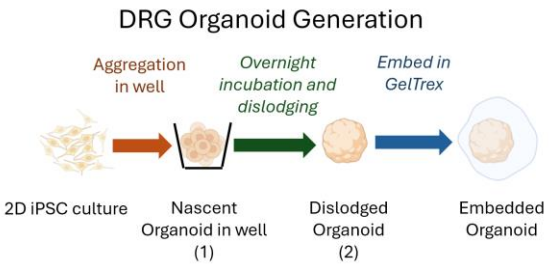

(B)

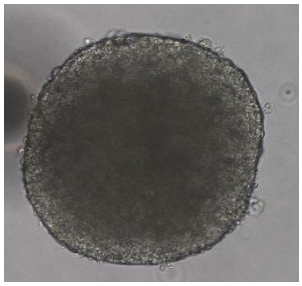

(C)

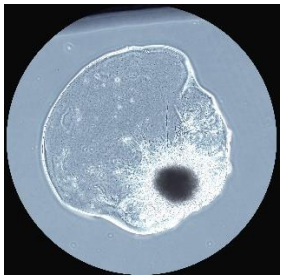

(D)

Figure 2. (**A**) A schematic showing the differentiation protocol of hDRG organoids for the first 24 days. Vertical gray lines indicate media changes. (**B**) A schematic showing the general approach to forming DRG organoids. (**C**) A d1 dislodged Regular condition organoid, 20x magnification. (**D**) A d19 Regular condition organoid, one week after embedding in Geltrex.

As established previously, the human dorsal root ganglion derives from the neural crest progenitor lineage. In order to pattern hiPSCs into this cell fate, the following morphogens and small molecules have been used to differentiate DRG cells (Cao et al.; Chambers et al.; Stacey et al.; Viventi et al). SB431542 ('SB') and LDN193189 ('LDN') are used to dually inhibit the SMAD signaling pathway, resulting in neuroectodermal differentiation. CHIR99021 ('CHIR') is a Wnt

signaling activator that promotes neural crest specification. N-[N-(3,5-Difluorophenacetyl)-L-alanyl]-S-phenylglycine t-butyl ester ('DAPT') is a Notch signaling inhibitor that facilitates neural differentiation by promoting cell cycle exit and maturation. SU5402 ('SU') is an FGFR inhibitor that suppresses FGF signaling, reinforcing neural crest commitment by limiting the expression of alternative mesodermal and endodermal differentiation pathways. Brain-derived neurotrophic factor ('BDNF') acts as a TRKB ligand, supporting the maintenance of mechanoreceptors by binding to TRKB receptors expressed by the same. Nerve growth factor ('NGF') is a TrkA ligand essential for the survival and maintenance of nociceptors by binding to TRKA receptors expressed by the same. Neurotrophin-3 ('NT3') serves as a TRKC ligand, promoting the maintenance of proprioceptors by binding to TRKC receptors expressed by the same. Glial cell line-derived neurotrophic factor ('GDNF') enhances mechanoreceptor differentiation, as demonstrated in previous studies (Viventi et al.). Lastly, ascorbic acid ('AA') stimulates neuronal differentiation by promoting an anterior neural fate. At day 12, DRG organoids are embedded in Geltrex (**Fig.3A**) (a solid medium to suspend organoids within) – to enable to the organoid's sensory neurons to have some physical medium within which to project their processes (**Fig. 3D**).

1.5. **Application of 5-fluorodeoxyuridine (FUDR)**

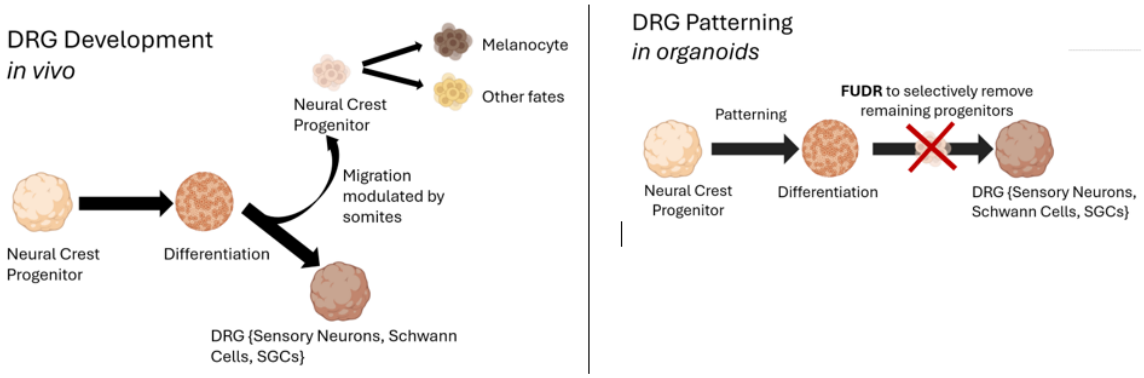

Figure 3. Schematic illustrating dynamics behind neural crest progenitors and DRG, made using BioRender.

As mentioned in section 1.2, DRG neurogenesis *in vivo* is followed by a further migration of neural crest progenitor cells induced by cues from somites, leaving behind a dorsal root ganglion with a lower level of neural crest progenitor cells (**Fig 1B**). The newly-formed neurons do not proliferate, while the remaining neural crest progenitors begin gliogenesis (Wiszniak and Schwarz). In organoids, once the process of gliogenesis has begun after neurogenesis is complete, we hypothesize that it is possible the non-neuronal cells will overgrow the neurons in the organoid and alter its function, absent some mechanism to arrest this gliogenesis. These cells could range from glia to other fates of the trunk neural crest cell lineage such as melanoblasts, chromaffin cells, glomus cells, and secretory cells of the endocrine system (Alhashem et al.; Achilleos et al,), given that differentiation *in vitro* is not as finely controlled as differentiation *in vivo* likely permitting a larger range of possible cell fates. This is important because the presence of non-neural or glial non-DRG cells would diminish the effectiveness of the organoid as an in vitro model of the DRG, as these additional non-native cells might alter functionality in unexpected ways. Additionally, the timing of this treatment may be important: different types of neurons are generated at different

times – Metzer presents one model for DRG development involving two distinct phases of neurogenesis initially believed to generate different cell types [Section 1.2.1]. This model is consistent with recent findings *in vivo* in mice and humans (Wiszniak and Schwarz; Lu, et al.). The interruption of differentiation after neurogenesis by an antimitotic agent might alter the relative composition of the neuronal population in the organoid as well if it prematurely interrupts the process of neurogenesis in between waves, though this is likely not a major factor to consider given the highly overlapping of these waves *in vivo*. The use of FUDR to the effect of terminating neural crest progenitor differentiation has been used in a previous study (Mazzara et al.). However, in vitro, a previous study generating DRG organoids from hiPSC lines have applied FUDR at day 17 and day 26, to this same stated purpose. This study found that two waves of neurogenesis occurred, with NEUROG1 expression peaking at around day 8 and NEUROG2 expression peaking at around day 30 (Lu, et al.)

1.5.1. FUDR's mechanism of action

FUDR inhibits thymidylate synthase (TS), which causes an imbalance of intracellular deoxyribonucleoside triphosphate (dNTP) pools – an imbalance which kills cells undergoing DNA replication, so behaving as an antimitotic agent. This is believed to be caused because the drug's downstream product, once synthesized, depletes intracellular thymine pools, leaving rapidly dividing cells unable to accurately replicate their DNA, leading to replication errors in the complementary strand and thus eventual cell death (Yoshioka et al.). During the differentiation of DRG organoids, a process that entails the phasing in and phasing out of media of various small molecules at various different time points, the addition of FUDR into the cell media in 2 doses (once at day 15 and once at day 22) (**Fig 2A**) serves to curb proliferative neural progenitor populations, mimicking their eventual migration out from the developing dorsal root ganglia *in*

vitro (**Fig 1B**) Neurons are not affected as they do not proliferate. The result is an organoid with relatively more neurons.

1.6. Neuronal Activity & Capsaicin

Neuronal activity is essential for validating the functional maturation of hiPSC-derived hDRG organoids, acting as a medium through which one may validate whether these cells can process and transmit sensory information like they would *in vivo*, validating their usefulness as models. If the neurons do not exhibit activity, it might suggest incomplete or incorrect differentiation or immaturity, making them ineffective for modelling sensory function. Voltage-gated ion channels play a critical role in generating electrical activity by regulating the generation and propagation of action potentials. Voltage-gated sodium channels, such as Nav1.7, Nav1.8, and Nav1.9, initiate action potentials and are essential for pain perception, with Nav1.7 being particularly important in human pain disorders. Assessing neuronal activity in DRG organoids involves electrophysiology techniques like patch-clamp recordings, calcium imaging to monitor intracellular signaling, and multi-electrode arrays (MEA) to track spontaneous and evoked firing patterns. The presence of functional voltage-gated ion channels and neuronal excitability confirms the maturity of DRG organoids, making them a physiologically relevant model for studying sensory processing through drug responses towards certain receptor agonists. The Transient Receptor Potential Vanilloid 1 (TRPV1) receptor, a receptor typically expressed on the cellular surfaces of nociceptors, is a non-selective polymodal receptor that is sensitive to acidic pH, temperature, endogenous lipids and capsaicin. *In vivo*, the first responses to capsaicin in DRG are detected at E12.5 in mice. Mouse E12.5 corresponds to roughly day 40 of human embryonic development (or what is known as Carnegie stage 16).

Capsaicin, a compound found in chili peppers, is responsible for sensation of spiciness, as it causes a burning sensation when it comes into contact with the skin or mucous membranes. It is of particular significance to this study as it is an agonist of the TRPV1 receptor, thus it can serve as an agonist for nociceptors to measure their activity (Frias et al.). Given that we are trying to investigate the activity of DRG neurons – which includes nociceptors, this compound is a useful agonist. Previous experiments in the lab have shown that peak response to capsaicin in our organoids, among those concentrations tested, has been seen at 3 μM capsaicin (Data Not Shown), hence this concentration was chosen to be used in this study.

2. Experimental Approach & Hypothesis

The experiment will consist of organoids (C4 line, d-1: 10/31/2024) belonging to three varying FUDR Treatment Groups, as listed below.

Treatment	*FUDR Application*	*Expected composition*
Regular FUDR	(d15, d22)	Neurons and glia in current observed ratio.
Later FUDR	(d29, d36)	Less neurons and more glia, due to additional time given to neural progenitors to proliferate.
No FUDR	None	Least neurons, most glia due to the most time given to neural progenitors to proliferate.

Table 1. The three recipes used in this study and their hypothesized effects on organoid patterning.

The characterization of the patterning and function of these conditions was carried out through a series of quantitative polymerase chain reaction (qPCR) assays and through measuring electrical activity using a microelectrode array (MEA).

3. Methods

3.1. Aggregation of hiPSC-derived organoids

Human induced pluripotent stem cells (hiPSCs, C4) were aggregated into 3D spheroids using AggreWell™800 plates (Stemcell Technologies, Cat. 34811). Prior to aggregation, hiPSC cultures were maintained in Essential 8 (E8) medium (ThermoFisher, Cat. A1517001) and passaged when confluent on 10 cm dishes. On the day prior to organoid differentiation (Day –1, 10/31/2024), the E8 medium was supplemented with 10 μM ROCK inhibitor Y-27632 (RI) (Tocris, Cat. 1254) and warmed to room temperature. Accutase (VWR, Cat. 10761-312) was also aliquoted (5 mL per 10 cm plate) and allowed to equilibrate at room temperature. AggreWell plates were prepared in a biosafety cabinet. 1 mL of Anti-Adherence Rinsing Solution (Stemcell, Cat. 07010) was added per well, followed by centrifugation at 1300 × g for 5 minutes. The rinsing solution was aspirated, and wells were washed twice with 1 mL DPBS (without Ca^{2+}/Mg). Media was aspirated from the hiPSC plates, and cells were incubated with 5 mL Accutase for 5 minutes at 37°C. Cells were then triturated off each plate using a 10 mL serological pipette by rinsing 2-3 times. The suspension was transferred to a 50 mL conical tube, and plate was additionally rinsed with an additional 5 mL of E8 + RI to collect remaining cells. The suspension (10 mL total) was centrifuged at 200 × g for 5 minutes. The supernatant was decanted, and the pellet was gently resuspended in 5 mL E8 + RI using a p1000. Cell viability and density were assessed using the Countess automated cell counter. A 1:1 mixture of cell suspension and Trypan Blue (5 μL each) was loaded into the Countess chamber, and live cell concentration was recorded. Based on this the suspension was diluted or concentrated as needed to achieve 1 mL per well in E8 + RI. 1 mL of the prepared cell suspension was added per well to deliver 3×10^6 cells per well. The plate was centrifuged at 200 × g for 5

minutes to distribute cells evenly into the microwells. Plates were then incubated for 24 hours at 37°C in a 5% CO_2 incubator to allow spheroid formation.

3.2. Dislodging of hiPSC-derived organoids

To dislodge and collect hiPSC-derived spheroids (**Fig 2C**) from AggreWell™800 plates, Essential 6 (E6) medium supplemented with Penicillin-Streptomycin (1:100; termed $E6^+$) was brought to room temperature within a biosafety cabinet. 3 ten-centimeter plates were pre-treated with 5 mL of Anti-Adherence Rinsing Solution (Stemcell, Cat. 07010) and set aside for use. A 70 μm cell strainer (Falcon, Cat. 35250) was placed into a 50 mL conical tube by the handle to maintain sterility. Spheroids were dislodged from the AggreWell microwells by pipetting the existing media up and down 5–6 times using a cut P1000 tip. The collected media, now containing a suspension of spheroids, was then passed through the cell strainer into the 50 mL conical tube. To retrieve any remaining organoids, each well was washed with 1 mL of DPBS without calcium and magnesium, and the rinse was also passed through the strainer. After aspirating the Anti-Adherence Rinsing Solution from the 10 cm plate, spheroids were transferred from the strainer into the plate by inverting the strainer and rinsing through its bottom with 1 mL of $E6^+$ medium supplemented with 0.5 μM Dorsomorphin (1:2000; Sigma, Cat. P5499-25MG) and 10 μM SB-431542 (1:1000; Selleck Chemicals, Cat. S1067). This step was repeated 2–3 times to ensure all trapped spheroids were dislodged into the culture plate. Additional $E6^+$ medium with Dorsomorphin and SB-431542 was added to bring the total volume in each plate to 10 mL. The 3 plates were assigned their respective conditions randomly and were then incubated at 37°C in a 5% CO_2 incubator.

3.3. Embedding of organoids

The organoids, which had begun patterning into hDRG, were embedded in Geltrex (Gibco™, Cat. A1413301) on day 12 of differentiation (11/11/2024). Plates were pre-treated by rinsing with 5 mL of Anti-Adherence Rinsing Solution (Stemcell Technologies, Cat. 07010), followed by a rinse with 5 mL of PBS. Plates were then filled with 12 mL of DRG media. 2.5 µL drops of Geltrex were pipetted onto a Parafilm sheet using a P2.5 pipette. The plate was placed in a 37°C incubator for 5 minutes to allow the drops to solidify. A total of 10–20 organoids were transferred into an Eppendorf tube using a cut P200 pipette tip. Media was carefully removed, and the organoids were resuspended in 100 µL of cold Geltrex. Using a P2.5 pipette with a cut tip, 2.5 µL of the organoid–Geltrex suspension, ideally with one organoid per drop (**Fig 2D**), was pipetted onto each pre-solidified Geltrex drop on the Parafilm. The parafilm was incubated for 5 minutes at 37°C to allow embedding. Following the initial embedding, an additional 2.5 µL drop of Geltrex was added on top of each organoid and allowed to solidify for another 5 minutes in the incubator. To transfer the embedded organoids, the Parafilm was held over a pre-warmed, media-filled 10 cm plate using forceps, and a P1000 pipette was used to gently wash the organoids off the Parafilm with culture media.

3.4. Patterning and Maintenance of Organoids

Organoids were kept in culture in 10 cm plates suspended in media. The composition, volume and frequency of replacing this media varied with time, but is available as supplementary information. **Figure 2A** showcases a general overview of the patterning process and media. Starting with day 12, the organoids receive Neurobasal-A (NBA) medium supplemented with 1:100 N2, 1:100 non-essential amino acids (NEAA), 20 ng/mL BDNF (1:1000), 200 µM ascorbic acid (1:1000), 10

ng/mL NT3 (1:2000), 20 ng/mL NGF (1:5000), and 20 ng/mL GDNF (1:5000) , hereafter known as DRG media. Media changes were conducted in biosafety hoods: the old media in each 10 cm plate was carefully aspirated out without aspirating organoids. Fresh media (12 or 15 mL, based on protocol) was then pipetted onto the plate, and the plate was returned to the incubator. For the Regular FUDR group, fresh DRG media was supplemented with FUDR at day 15 and day 22. For the Delayed FUDR group, fresh DRG media was supplemented with FUDR at day 29 and day 36. For the No FUDR group, FUDR was never supplemented during any media change. For each application of FUDR, organoids were exposed for around 24 hours when the supplemented DRG media was replaced with fresh DRG media the next day.

3.5. RNA extraction and cDNA synthesis

For quantitative PCR (qPCR) analysis, organoids were collected at days 25, 63, and 102 of differentiation. At each time point, three organoids per experimental condition were harvested for RNA extraction. Total RNA, including microRNA, was isolated using the miRNeasy Mini Kit (Qiagen, Cat. 217084), which utilizes QIAzol-based microRNA purification. RNA extraction was carried out according to the manufacturer's protocol. Complementary DNA (cDNA) synthesis was performed on the previously extracted RNA samples using the Maxima First Strand cDNA Synthesis Kit for RT-qPCR (Thermo Fisher Scientific, Cat. No. K1641).

3.6. qPCR analysis

Reactions were prepared using a SYBR Green-based master mix according to the manufacturer's instructions. The qPCR was conducted on a QuantStudio™ Real-Time PCR System (Applied Biosystems), with cycling conditions as follows: an initial activation step at 95°C for 10 minutes,

followed by 40 cycles of denaturation at 95°C for 1:20 seconds and annealing/extension at 60°C for 60 seconds. A melt curve analysis was performed to confirm the specificity of amplification.

Data acquisition and analysis were carried out using QuantStudio™ Design and Analysis Software v2.8. Threshold cycle (Ct) values were determined automatically by the software, and relative gene expression levels were calculated using the ΔΔCt method, normalizing target gene expression to β-actin and comparing across experimental conditions.

The following table lists the primers used in this analysis:

Gene	Marker of…	Source
SOX10	Neural crest progenitors	Metzer et al.
BRN3A	DRG progenitors	Qi et al.
ISL1	Neuronal DRG marker (though some sources claim it's a motor neuron marker?)	Qi et al.
TRKA/TRKB/TRKC	Neuronal DRG marker for each respective sensory neuron (nociceptor/ mechanoreceptor / proprioceptor)	Metzer et al.
MBP	Satellite glial cell and Schwann cell marker	Liu et al.
FABP7	SGC specific marker	Avraham et al.
OCT4	Schwann cell marker	Liu et al.
MART-1	Melanoblast lineage marker	Kulesa et al.
PTGES3	Gene linked to PGE2 expression	Kantarci et al.
GFAP	Astrocyte activation	Liu et al.

Table 2. qPCR panel of genes used in this study

Results were obtained using relative quantification (RQ) values normalized to β-actin. For each gene, RQ per biological replicate wars calculated as the mean of two technical replicates. Final RQ values per condition and timepoint represent the mean of three biological replicates, and for certain genes, the plotted error bars indicate the standard deviation across biological replicates.

Additionally, a volcano plot was constructed. This was done by calculating the log-fold change per gene as

$$Log2FC = log_2(\frac{RQ(Condition)}{RQ(Regular)})$$

while p-values were calculated comparing the 3 biological replicate RQ values per condition per gene using an independent t-test.

3.7. MEA

Electrophysiological recordings were conducted using the Accura-3D microelectrode array (MEA) system (3Brain AG), which features a high-density 3D-based architecture specifically designed for interfacing with three-dimensional neuronal cultures and organoids. Chip set up and inter-session cleanings were performed according to the manufacturer's protocol provided by 3Brain AG Organoids were transferred to the MEA chip and allowed to equilibrate in culture medium for 5 minutes in 1 mL of DRG media prior to recording. Chips were maintained at 37°C with 5% CO_2 using the system's environmental control unit throughout the recording session. 6 organoids per condition were recorded. Each organoid was allowed 5 minutes to acclimate to the new chip environment, then spontaneous activity was recorded for 5 minutes ('Baseline'). Subsequently, 1 µL of 3 mM capsaicin stock in DMSO was added to the well to bring it to 3 µM capsaicin. The organoid was left to acclimate for 2 minutes, then was recorded again for 5 minutes ('Capsaicin'). Recordings were performed using the integrated BioCAM X platform (3Brain AG), and data were acquired using BrainWave software, with further data analysis performed in Microsoft excel and Python JupyterLab.

4. Results

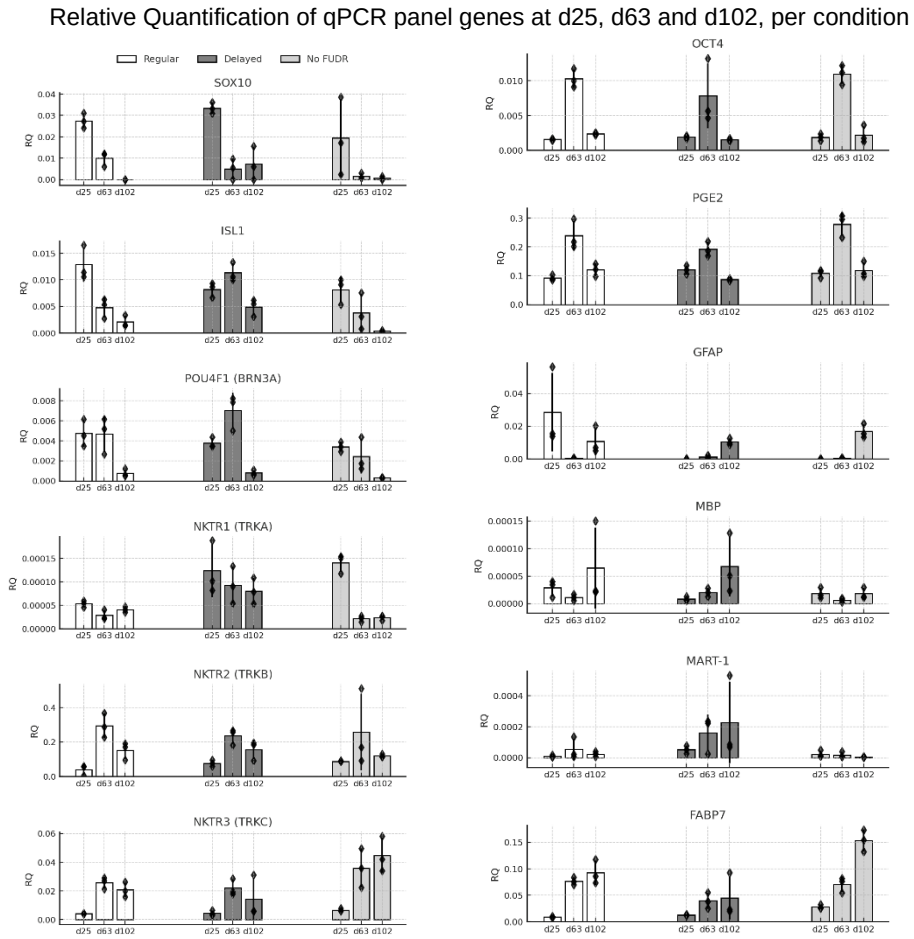

(A)

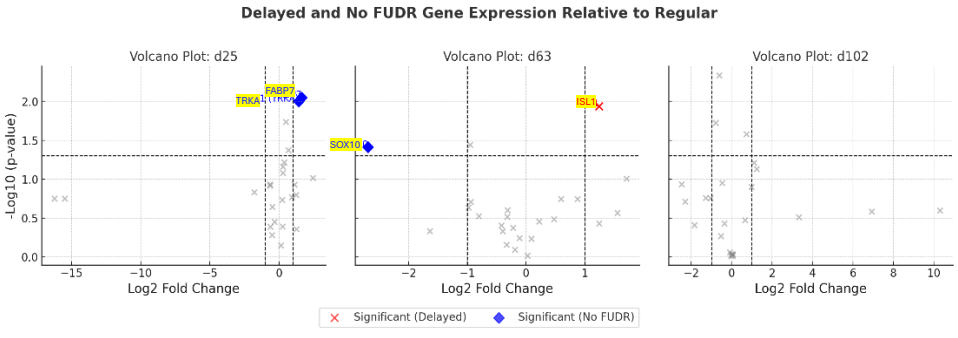

(B)

Figure 4. (A) Bar plots showing relative quantification (RQ) of selected genes normalized to β-actin across three developmental timepoints (d25, d63, d102) and three experimental conditions (Regular, Delayed, and No FUDR). Individual RQ values for biological replicates are displayed as black diamonds. Error bars indicate the standard deviation across biological replicates. **(B)** Delayed and No FUDR gene expression relative to Regular conditions at three different time points (d25, d63, and d102). The x-axis represents the Log2 Fold Change (Log2FC), and the y-axis represents the -Log10 (p-value)

qPCR assays show differences of certain genes, among treatment groups

In order to understand the cellular composition of each recipe, we performed a gene expression analysis using qPCR for a panel of genes associated with the range of cellular fates hypothesized to be present in our DRG organoid (**Table 2**). As stated previously, results were obtained using relative quantification (RQ) values normalized to β-actin.

At d102. *TRKB a*nd *FABP7* relative quantification was higher in the No FUDR condition (**Fig 4A**), while *TRKA* and *ISL1* RQ were highest in Delayed FUDR for the same time points. The most significant between-condition gene differences were the upregulation of *FABP7* and *TRKA* in the Delayed condition relative to the Regular condition at day 25, the downregulation of *SOX10* in the No FUDR condition relative to the Regular condition at day 63 and the upregulation of *ISL1* in the Delayed condition relative to Regular condition at day 63 (**Fig. 4B**).

qPCR show that some genes consistently change with time across conditions.

We chose to investigate whether expressions of genes change with time, as would be expected of our model of patterning. The relative quantification of *TRKA* and *SOX10* was highest for all conditions at the d25 timepoint (**Fig. 4A,**). The relative quantification of *TRKB*, *BRN3A* and *PGE2* was similarly highest for all conditions at the d63 timepoint (**Fig. 4A**). *FAPB7* RQ was highest for all groups at the d102 timepoint (**Fig. 4A**). In contrast, the relative quantification of *TRKC* peaks at d63 for both the regular and delayed conditions, but peaks at d102 for the No FUDR condition. *ISL1* RQ peaks for the regular and No FUDR groups at d25 and declines, but is at its maximum at the d63 time point for the Delayed FUDR group. The expression of other non-neuronal cell markers *OCT4* and *PGE2* peaked at d63. The expression of astrocyte and glial cell markers like

GFAP, *MBP* and *FABP7* peaked at day 102. The expression patterns of neuronal markers such as *BRN3A*, *TRKA*, *TRKB* and *TRKC* was variable (**Fig. 4A**).

Figure 5

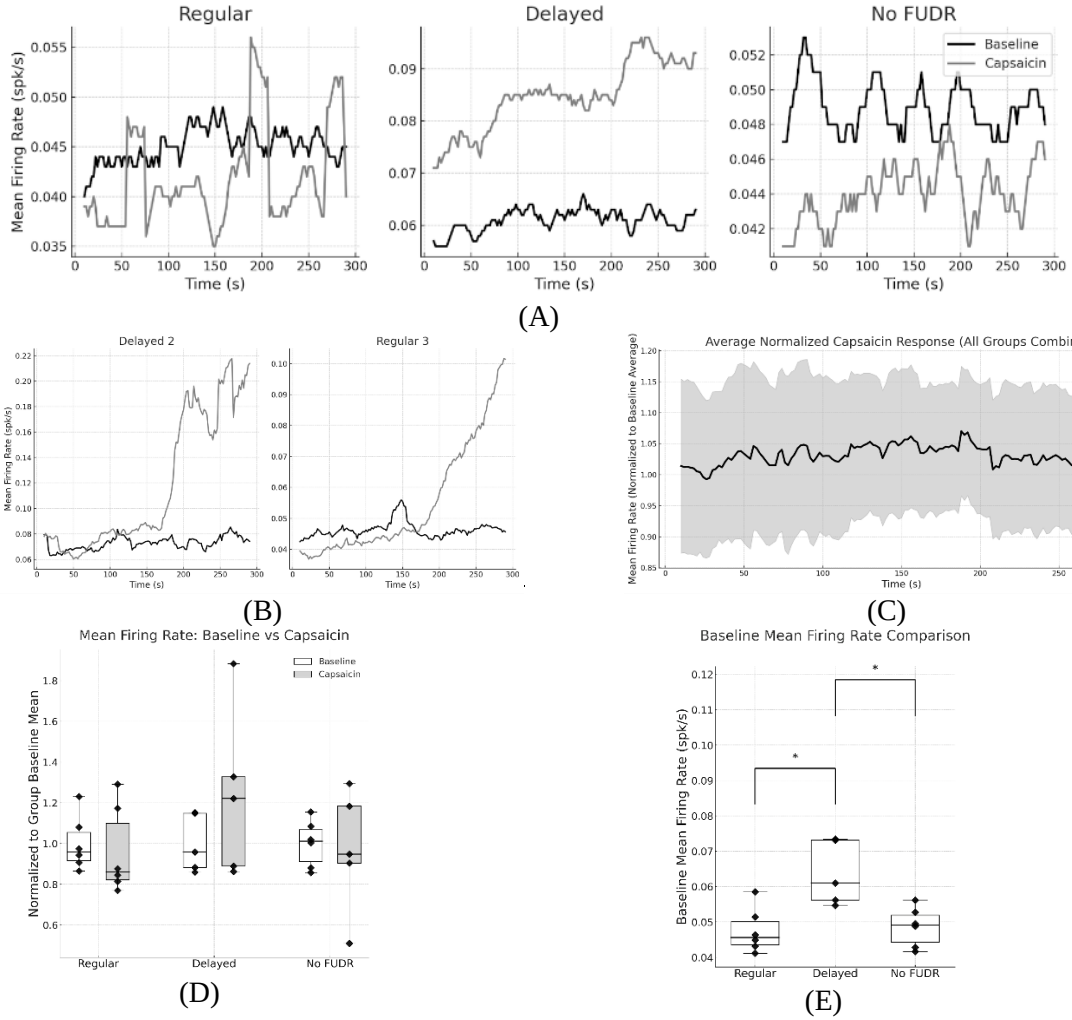

Figure 5. **(A)** Side-by-side plots showing the mean firing rate (MFR) of 3 representative organoids during baseline and after the application of 3 µM capsaicin. The data were smoothed using a rolling window of 10 time points. Mean firing rate at time *t* was calculated as the average of the firing rate of all electrodes at that time *t*. **(B)** Side-by-side plots showing the mean firing rate (MFR) of Delayed 2 (left) and Regular 3 (right) organoids during baseline and after the application of 3 µM capsaicin. The data were smoothed using a rolling window of 10 time points. **(C)** Plot showing the average normalized mean firing rate (MFR) over time in response to 3 µM capsaicin across Regular, Delayed, and No FUDR groups. Each group's response is averaged across organoids within the condition, and the shaded area represents the 95% confidence interval. The data were smoothed using a rolling window of 10 time points. **(D)** Box-and-whisker plot showing the distribution of baseline mean firing rates (MFR) for Regular, Delayed, and No FUDR groups. Pairwise t-tests yielded no significant differences between baseline & capsaicin for any condition. **(E)** Box-and-whisker plot showing the distribution of baseline mean firing rates (MFR) for Regular, Delayed, and No FUDR groups. Statistical significance at alpha = 0.05 is indicated by the brackets.

Conditions statistically significantly differ in their spontaneous MEA baseline activity

As stated prior, it is important our recipe produces active neurons that can be assessed in future studies. To this effect, we chose to analyze the baseline mean firing rate (MFR) of our organoids as a measure of neuronal activity. To assess baseline activity across experimental groups, the mean baseline MFR was calculated for each organoid. These values were compared between the Regular, Delayed, and No FUDR groups using unpaired two-tailed t-tests. One outlier (Delayed 6) with a substantially elevated MFR was excluded to reduce skew. Significant differences were observed between Regular and Delayed ($p = 0.012$), and between Delayed and No FUDR ($p = 0.016$). No significant difference was found between Regular and No FUDR ($p = 0.770$). (**Fig. 5E**).

MEA shows variable peak responses to capsaicin

To investigate and compare the activity of neurons resulting from our three recipes, the electrical activity of an organoid was recorded via MEA chip for 5 minutes during a baseline and a 3 μM capsaicin recording. To quantify the activity of the organoid, the mean firing rate (MFR) was used as the variable of interest. Over the 5 minute recording, mean firing rate at time t was calculated as the average of the firing rate of all electrodes touching the organoid at that time t, where firing rate was calculated using time bins of 2 seconds. To plot the changes in firing rate over time, a rolling window of 10 units was used to plot MFR, such that the MFR at t was calculated as the average of the MFR over the range [t-5, t+5]. This choice of window was arbitrary.

In order to gauge the level of nociceptor activity via change in electrical activity upon exposure to capsaicin, we had to analyze the capsaicin response relative to the baseline. Before we could do this, we had to choose an appropriate time window to deem the capsaicin ‘response’ time – if the recording lasted too long, the capsaicin response would diminish with time and negatively

skew our results. If the recording was too short, the capsaicin response might not reach its peak and similarly negatively skew our results. Across conditions and replicates, mean firing rate responded in variable ways to the addition of 3 μM capsaicin. For the duration of the recording, the capsaicin mean firing rate stayed consistently higher for some organoids (**Fig. 5A, center**), was consistently lower than the baseline for some replicates (**Fig. 5A, right**) and was variable relative to the baseline for others (**Fig. 5A, left**). For two replicates, baseline activity started higher than capsaicin response, before capsaicin mean firing rate began to consistently increase near the end of the recording (**Fig. 5B**). Because of the indication that capsaicin response might not be efficiently captured under current protocol due to the visual appearance of certain responses (**Fig. 5B**), analysis was performed to see if this was a general trend or not. Capsaicin firing rates per organoid were normalized as a fraction of the overall mean firing rate of their baseline recordings. Then, the average normalized 5 minute capsaicin response of the 17 replicates (one could not be used due to a file corruption) was plotted against time, with 95% confidence intervals (**Fig. 5C**). The generalized response shows a response to capsaicin centered around 1.00 x Baseline MFR, with a generally uniform distribution across the 5 minute interval.

MEA analysis reveals no statistically significant general response to capsaicin

In order to investigate nociceptor activity in particular, we chose to expose organoids to the TRPV1 agonist capsaicin at 3 μM concentration, in order to measure change in electrical activity as a proxy measure of nociceptor activity in the organoid under the assumption that specifically any nociceptors present would express the *TRPV1* receptor and would respond to capsaicin. The average baseline MFR (averaged per organoid over the period of the five minute recording) for the 5 to 6 replicates of each condition were further averaged to produce a pooled baseline average MFR for each condition. Then, the average capsaicin MFR for the same replicates was normalized

as a fraction of this average, and a box and whisker plot was performed. Organoid per condition were normalized to their pooled average rather than individual averages to enable statistical tests between baseline and capsaicin recordings – normalizing each replicate's average MFR to itself would result in a baseline distribution with no variation, precluding the possibility of a statistical test. A box and whisker plot was constructed (**Fig. 5D**) Paired t-tests yielded no significant differences between baseline and capsaicin for any condition.

Capsaicin response is variable among firing neurons

We chose to analyze the patterns of capsaicin response among our recipes in further detail to see if, despite no significant differences in MFR, it was possible that the capsaicin response varied in other ways. If this was the case, we could still conclude useful information about the nature of electrical activity, and thus neurons, across the three condition. This is because, while we found that capsaicin response is variable and generally not significantly different from baseline response (**Fig. 5D**), the mechanism behind why could still differ among the recipes. There are generally two potential different mechanisms that would yield identical MFRs of 0. First, it is possible that neurons exhibit strong and consistent baseline activity, activity that does not change in response to capsaicin, yielding a change of zero as the capsaicin and baseline firing rates are identical. The second is that neurons do have a differential response in their firing rate upon exposure to capsaicin, but the way these changes manifest results in a net change of 0.

Given that MFR of an organoid at time *t* is calculated as the average of the firing rate across all electrodes, a change in MFR of 0 might be caused by no change in the electrodes' firing rates as described previously if neurons do not change their firing rate at all. Alternatively, it is possible that the net change in firing rate cancel each other out yielding a change in MFR of zero. There are two ways this could happen. If one population / subtype of neurons consistently increased their

firing rates due to capsaicin while the other decreased firing rates due to desensitization, and these changes were of the same magnitude, then the change in MFR of 0 might conceal a tangible response to capsaicin. This is a possibility as the exposure of neurons to capsaicin in the organoid model is likely not homogenous, as neurons near the outer edge are likely to be exposed to capsaicin for longer times and potentially higher concentrations than neurons embedded deep within the geltrex. Alternatively, it could be a product of spontaneous activity: if activity is truly spontaneous, we might expect changes in the firing rate of electrons to also be random. This could happen if the capsaicin no effect and was functionally like another replicate recording of spontaneous activity. Spontaneous activity is random, so the distribution of capsaicin electrode firing rates is independent of the distribution of baseline electrode firing rates, yielding a net change of zero if both distributions are centered around the same baseline mean firing rate.

To investigate this possibility, we constructed heat maps depicting the spatial distribution of the change in mean firing rate, relative to the baseline upon addition of 3 μM capsaicin. Only electrodes upon which the organoid was directly resting upon were included. Dashed outlines mark the shape of the organoid. Color scale clipped at ±0.1 spk/s to highlight subtle modulation.

Figure 6

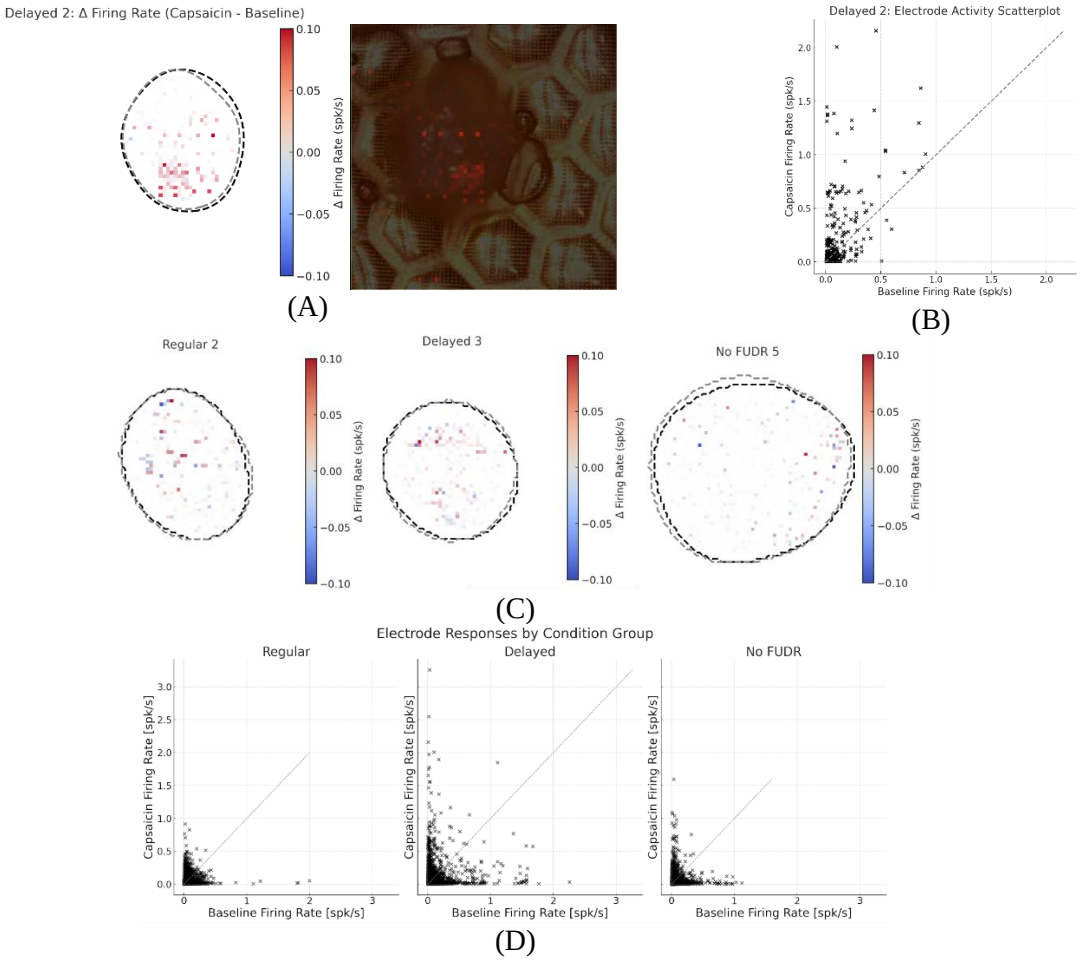

Figure 6. **(A)** A heat map depicting the spatial distribution of the change in mean firing rate, relative to the baseline, seen in the Delayed 2 organoid upon addition of 3 µM capsaicin. Only electrodes upon which the organoid was directly resting upon were included. Dashed outlines mark the shape of the organoid. Color scale clipped at ±0.1 spk/s to highlight subtle modulation. An actual picture of the organoid included for reference. **(B)** Scatterplot of average firing rates for each electrode under baseline and 3 µM capsaicin conditions in the Delayed 2 organoid. Each point represents an individual electrode. **(C)** Heatmaps showing the change in overall mean firing rate following the addition of 3 µM capsaicin in three organoid replicates: Regular 2, Delayed 3, and No FUDR 5. **(D)** Pooled scatterplots of average firing rates for each electrode under baseline and 3 µM capsaicin conditions for all replicates, grouped by condition.

Such heatmaps showcase how the variable responses to capsaicin manifest: the heatmap of the organoid in **Fig. 5C**, Delayed 2, showed a generally consistent increase in firing rate (**Fig. 6A**) in the center of the organoid. The representative organoids from **Fig. 5A** showed heatmaps with evenly distributed positive and negative changes (**Fig. 6A**). In order to quantify the overall distribution of these changes, a scatterplot of average firing rates for each electrode under baseline

and 3 μM capsaicin conditions were created. (**Fig. 6B, D**). The Delayed 2 organoid shows a population of electrodes with high firing rates that further increased when capsaicin was administered (**Fig. 6B**). Pooled scatter graphs, for all organoids across conditions, showcase slightly different distributions.

5. **Discussion**

Here we aimed to characterize a recipe to generate DRG organoids from hiPSCs. DRG somatosensory neurons and non-neuronal cells are generated from the neural crest during development, along with other cells such as melanocytes and glia such as astrocytes and Schwann cells (Alhashem et al.). Previous studies have shown that neurogenesis and generation of sensory DRG neurons in vitro is followed by generation of glial cells and other non-neural cells. We want to find a recipe that exhibits distributions of cell types identical to the human embryonic DRG. While we might directly compare these recipes to the distributions of embryonic DRG cells, this is an expensive process. Before we might undergo such a step, we require a recipe that is reliable, consistently produces populations of active neurons – the cells of interest in our research, and that has been tested such that the effect of altering components of the recipe has already been tested in case methods such as single cell RNA sequencing show pertinent differences between embryonic tissue and our recipe. To lay down the foundations of this process, we tested different FUDR treatments to stop proliferation of neural crest progenitor cells at different time points of the differentiation process. We hypothesized that this would change the composition/proportions of cells within our organoids. To test this we did quantitative polymerase chain reaction (qPCR) assays to investigate overall markers of cell identity within our organoids. Additionally, to the effect of producing a recipe that produces active neurons, we performed microelectrode assays (MEA) to measure levels of electrical activity within our organoids across the three recipes tested.

We found that overall, the relative levels of gene expression with respect to identity and time match the biological model of DRG development for all three recipes. With respect neuronal activity, we found differential results among our three conditions.

qPCR results show evidence of a wave of neurogenesis and a gliogenic switch

The expression patterns of various genes serve as potential evidence of demonstrating the occurrence of the gliogenic switch in this hDRG organoid model. Neural progenitor genes, such as SOX10, are high at d25 but quickly fall in their relative quantification (RQ) as time progresses. (**Fig. 4A**). Conversely, glial cell markers such as *FABP7*, *MBP* and *GFAP* tend to increase as time progresses, with most replicates at their highest RQ at the d102 timepoint (with the exception of an outlier for d25 Regular *GFAP*) (**Fig. 4C**). This switch from neural progenitor marker expression to glial marker progression mirrors what occurs in vivo when the gliogenic switch occurs at around gestation week 12 and studies have found that this switch occurs in DRG organoids by day 60, supporting the validity of our organoids to model embryonic dorsal root ganglion tissue (Lu, et al.). Additionally, the patterns of gene expression support the validity of our initial hypothesis of how FUDR affects DRG organoids, given that the glial marker *FABP7* was significantly upregulated in the No FUDR at the day 63 timepoint relative to the Regular condition (**Fig. 4C**). For the regular and delayed groups, the consistent maximum RQ of neuronal markers such as *ISL1*, *TRKB* and *TRKC* at the d62 timepoint, and later fall at the d102 timepoint strengthens this claim (**Fig. 4A**), supporting the idea that in between neural crest differentiation and gliogenesis, there is a wave of neurogenesis. Taken together, these qPCR results match our hypothesized model of differentiation and patterning in our organoids (**Fig. 3A, 4A**).

Delayed FUDR application may arrest neurogenesis closer to the gliogenic switch

Based on the increased baseline electrical activity of delayed FUDR organoids (**Fig.5E**), and their relatively elevated levels of ISL1 at the d62 and d102 timepoints (**Fig. 4C.**), one could hypothesize that a delayed FUDR treatment may be more effective by arresting progenitor cell division after more neurogenesis has been allowed to take place. At d25, ISL1 RQ has peaked for the regular FUDR group, which has already been treated with FUDR at this point. At d63, the ISL1 for the Delayed FUDR group has increased compared to d25 (**Fig. 4C.**), indicating that additional neurogenesis has occurred at some time between these timepoints that did not occur for the Regular FUDR group. One could argue that the decrease of d63 ISL1 in the No FUDR group invalidates this claim as it should have had the same opportunity to undergo additional neurogenesis, but it could be argued that by d63, the No FUDR group has undergone the gliogenic switch and the relative level of neurons in the organoids has begun to decrease as other cells proliferate, lowering the RQ – this could be considered be consistent with the higher RQs of glial markers such as Fabp7 and PGE2 (produced by Schwann cells) in No FUDR d63 compared to Delayed FUDR d63 (**Fig. 4C.**). Anecdotally speaking, No FUDR organoids tended to be of a larger size than the other conditions, as evident in **Fig. 6C**. The low variability of ISL1 RQ values across all three conditions and timepoints lends further credence to this claim (**Fig. 4C.**). Based on these results, it's likely that this gliogenic switch likely occurs between d25 and d63.

Delayed FUDR's increased baseline electrical activity may be explained by non-nociceptor neurons

MEA results show that in general, mean firing rates did not differ significantly upon addition of 3 μM capsaicin for any group (**Fig. 5D**). The increased baseline activity of the Delayed FUDR group can be seen in the scatterplots, where the distribution of firing rates for this group is more spread

out. This indicates that the Delayed FUDR group tended to have more electrodes that had higher firing rates (**Fig. 6D**), indicating either a higher density of neurons or a larger fraction of neuronal population. qPCR results can help explain the higher activity but lack of response: TrkB and ISL-1 relative quantifications for the Delayed FUDR group are higher than the other groups at d102, which is close to our MEA timepoint of d120 (**Fig. 4C**). In contrast, while TrkA is also highest for Delayed FUDR at d102, the RQ of this gene is orders of magnitude lower than the RQ for the other neuronal markers (**Fig. 4C**). Therefore, it could be argued that this is evidence that Delayed FUDR has more neurons than the other groups, but that these neurons are not nociceptors. This is consistent with the MEA results (**Fig. 5D, E**). The lack of a consistent increase in capsaicin firing rate but the strong presence of a high level of baseline activity might suggest that it is neurons that are not sensitive to capsaicin (ie, non-nociceptors) that might be responsible for this observation. Additionally, because PGE2 expression did not differ significant between groups at any time point (**Fig. 4A, B**), we can likely rule out the effects of PGE2 inducing hyperexcitability in the Delayed FUDR group as the explanation behind this condition's elevated baseline firing rates. However, further studies would be required to definitively show this by comparing activity across PGE2 and PGE2 knockout conditions, for example.

6. Conclusions & Future Directions

qPCR validates the recipes as an *in vitro* model of DRG development *in vivo*.

Gene expression patterns were consistent with what one might expect from a wave of neurogenesis followed by a gliogenic switch. Neural progenitor markers such as SOX10 were highly expressed early (d25), while glial markers such as FABP7 and GFAP peaked at later timepoints (d102), reflecting expected lineage progression. These results are in line with results found by Lu et al., who performed similar analyses with hiPSC derived DRG organoids. Future directions for comparing this model to the embryonic human DRG may include bulk or single cell RNA seq to compare the gen expression profiles of these recipes to embryonic human DRG to gauge the level of similarity.

Delayed FUDR May Arrest Neurogenesis Closer to the Gliogenic Switch

qPCR and MEA results seem to support the hypothesis that Delayed FUDR may be more effective by allowing more time for neurogenesis to occur before arresting progenitor cell division, leading to increased baseline neuronal activity. However several avenues remain unexplored: most crucially, investigating the expression of genes that mark neurogenesis such as *NEUROG1* and *NEUROG2* may yield crucial evidence for or against the conclusions presented in this paper. Additionally, more qPCR analysis for additional markers of non-glial and non-neuronal neural crest lineage cells is required, as the identity of the No FUDR group still remains mostly unknown.

Immunohistochemistry can help contextualize relative quantifications

Much of the analysis in this paper relies on comparing RQs of genes across conditions. However, the relative quantification of a gene is not a strict measure of its absolute expression – the low

TrkA RQ might be due to low TrkA expression or might simply be because TrkA requires little mRNA to be expressed highly. To mitigate this confounding variable, immunostains of organoids with these markers would be a highly useful tool to contextualize what these RQs mean.

7. Limitations

Only one differentiation of one hiPSC line was used in this analysis

It is well known that organoids tend to not only have a high degree of line-to-line variability, but also differentiation-to-differentiation variability. Repeating this experiment across another differentiation would be very useful in determining whether the trend holds or not, which would be crucial in determining the reproducibility of these results.

Lack of an earlier timepoint is a confounding variable for qPCR

A big confounding variable limiting the statistical power of the qPCR results is the lack of a qPCR timepoint before d15 – when the Regular FUDR group was treated with FUDR. If this existed, and if the RQs of all genes were roughly similar to each other at this time point, then one could be confident in saying that subsequent changes between groups were causally linked to the FUDR treatment. Additionally, the number of qPCR timepoints could be increased to see RQ trends in finer detail and the analysis could be made more robust by having included a d120 qPCR timepoint, which would have helped solidify the links between qPCR results and MEA results.

Variability in MEA could be due to Geltrex

There is a high degree of variability in the MEA results – this could be due to organoid variability, but this could also be due to external factors like how the organoid lands on the MEA chip. DRG organoids are embedded in Geltrex, with the actual spheroid rarely perfectly enveloped in the Geltrex, or with more than one spheroid in the Geltrex (**Fig. 3D**). If the Geltrex does not contribute to electrical activity, then an organoid that lands with the Geltrex facing the electrodes will have a lower measured activity than if the same organoid has the spheroid directly touching the electrode. To balance this effect, a relatively larger n of 6 per condition was used.

References

1. Achilleos, Annita, and Paul A. Trainor. "Neural crest stem cells: discovery, properties and potential for therapy." *Cell research* 22.2 (2012): 288-304.
2. Alhashem, Zain, et al. "Trunk Neural Crest Migratory Position and Asymmetric Division Predict Terminal Differentiation." *Frontiers in Cell and Developmental Biology*, vol. 10, article no. 887393, 2022, https://doi.org/10.3389/fcell.2022.887393.
3. Avraham, Oshri, et al. "Profiling the molecular signature of satellite glial cells at the single cell level reveals high similarities between rodent and human." *Pain*, vol. 163, no. 12, 2022, pp. 2348-2364. https://doi.org/10.1097/j.pain.0000000000002628.
4. Cao, Lishuang, et al. "Pharmacological reversal of a pain phenotype in iPSC-derived sensory neurons and patients with inherited erythromelalgia." *Science translational medicine* 8.335 (2016): 335ra56-335ra56.
5. Chambers, Stuart M., et al. "Combined small-molecule inhibition accelerates developmental timing and converts human pluripotent stem cells into nociceptors." *Nature biotechnology* 30.7 (2012): 715-720.
6. Frias, Bárbara, and Adalberto Merighi. "Capsaicin, nociception and pain." *Molecules* 21.6 (2016): 797.
7. Ho, Beatrice Xuan, et al. "Disease Modeling Using 3D Organoids Derived from Human Induced Pluripotent Stem Cells." *International Journal of Molecular Sciences*, vol. 19, no. 4, 2018, article no. 936, https://doi.org/10.3390/ijms19040936.
8. Jean, Ying Y., et al. "Glutamate elicits release of BDNF from basal forebrain astrocytes in a process dependent on metabotropic receptors and the PLC pathway." *Neuron Glia Biology*, vol. 4, no. 1, 2008, pp. 35-42. Cambridge University Press, doi:10.1017/S1740925X09000052.
9. Jung, Min, et al. "Cross-species transcriptomic atlas of dorsal root ganglia reveals species-specific programs for sensory function." *Nature Communications*, vol. 14, article no. 366, 2023, https://www.nature.com/articles/s41467-023-36014-0.
10. Kantarci, Husniye, et al. "Schwann cell-secreted PGE_2 promotes sensory neuron excitability during development." *Cell*, vol. 187, no. 17, 2024, pp. 4690-4712.e30. doi:10.1016/j.cell.2024.07.033.
11. Koeppen, A. H., et al. "The dorsal root ganglion in Friedreich's ataxia." *Acta Neuropathologica*, vol. 118, no. 6, 2009, pp. 763-776. doi:10.1007/s00401-009-0589-x.
12. Kulesa, Paul M., et al. "Reprogramming Metastatic Melanoma Cells to Assume a Neural Crest Cell-Like Phenotype in an Embryonic Microenvironment." *Proceedings of the National Academy of Sciences of the United States of America*, vol. 103, no. 10, 2006, pp. 3752-3757. https://doi.org/10.1073/pnas.0506977103.
13. Liu, Zhangyin, et al. "Specific Marker Expression and Cell State of Schwann Cells during Culture In Vitro." *PLOS ONE*, vol. 10, no. 4, 2015, article e0123278, https://doi.org/10.1371/journal.pone.0123278.
14. Lu, Tian, et al. "Decoding transcriptional identity in developing human sensory neurons and organoid modeling." *Cell* 187.26 (2024): 7374-7393.

15. Ma, Qiufu, et al. "NEUROGENIN1 and NEUROGENIN2 control two distinct waves of neurogenesis in developing dorsal root ganglia." *Genes & Development*, vol. 13, no. 13, 1999, pp. 1717-1728. https://doi.org/10.1101/gad.13.13.1717.

16. Mazzara, Pietro Giuseppe, et al. "Frataxin gene editing rescues Friedreich's ataxia pathology in dorsal root ganglia organoid-derived sensory neurons." *Nature Communications* 11.1 (2020): 4178.

17. Meltzer, Shan, et al. "The cellular and molecular basis of somatosensory neuron development." *Neuron*, vol. 109, no. 23, 2021, pp. 3736-3757.

18. Morrison, Sean J., et al. "Transient Notch Activation Initiates an Irreversible Switch from Neurogenesis to Gliogenesis by Neural Crest Stem Cells." *Cell*, vol. 101, no. 5, 2000, pp. 499-510. https://doi.org/10.1016/S0092-8674(00)80860-0.

19. Qi, Yuchen, et al. "Combined small-molecule inhibition accelerates the derivation of functional cortical neurons from human pluripotent stem cells." *Nature Biotechnology*, vol. 35, no. 2, 2017, pp. 154-163.

20. Shiers, Stephanie, et al. "Quantitative differences in neuronal subpopulations between mouse and human dorsal root ganglia demonstrated with RNAscope in situ hybridization." *Pain*, vol. 161, no. 10, 2020, pp. 2410-2424. doi:10.1097/j.pain.0000000000001973.

21. Stacey, Peter, et al. "Plate-based phenotypic screening for pain using human iPSC-derived sensory neurons." *SLAS DISCOVERY: Advancing Life Sciences R&D* 23.6 (2018): 585-596.

22. Viventi, Serena, and Mirella Dottori. "Modelling the dorsal root ganglia using human pluripotent stem cells: A platform to study peripheral neuropathies." *The International Journal of Biochemistry & Cell Biology*, vol. 100, 2018, pp. 61-68.

23. Wiszniak, Sophie, and Quenten Schwarz. "Notch signalling defines dorsal root ganglia neuroglial fate choice during early neural crest cell migration." *BMC Neuroscience*, vol. 20, article no. 21, 2019, https://bmcneurosci.biomedcentral.com/articles/10.1186/s12868-019-0501-0.

24. Yoshioka, Akiko, et al. "Deoxyribonucleoside Triphosphate Imbalance: 5-Fluorodeoxyuridine-Induced DNA Double Strand Breaks in Mouse FM3A Cells and the Mechanism of Cell Death." *The Journal of Biological Chemistry*, vol. 262, no. 17, 1987, pp. 8235-8241, https://www.jbc.org/article/S0021-9258(18)47554-0/pdf.